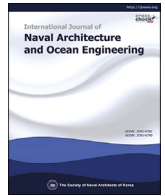




Contents lists available at ScienceDirect

International Journal of Naval Architecture and Ocean Engineering

journal homepage: <http://www.journals.elsevier.com/international-journal-of-naval-architecture-and-ocean-engineering/>

Numerical studies on non-linearity of added resistance and ship motions of KVLCC2 in short and long waves



Olgun Hizir^{a,*}, Mingyu Kim^a, Osman Turan^a, Alexander Day^a, Atilla Incecik^a, Yongwon Lee^b

^a Department of Naval Architecture, Ocean and Marine Engineering, University of Strathclyde, 100 Montrose Street, Glasgow, G4 0LZ, UK

^b Global Technology Centre, Lloyd's Register, Southampton, SO16 7QF, UK

ARTICLE INFO

Article history:

Received 30 March 2017
Received in revised form
23 February 2018
Accepted 27 February 2018
Available online 21 March 2018

Keywords:

Added resistance
Wave steepness
Short waves
Potential flow
CFD
KVLCC2

ABSTRACT

In this study, numerical simulations for the prediction of added resistance for KVLCC2 with varying wave steepness are performed using a Computational Fluid Dynamics (CFD) method and a 3-D linear potential method, and then the non-linearities of added resistance and ship motions are investigated in regular short and long waves. Firstly, grid convergence tests in short and long waves are carried out to establish an optimal mesh system for CFD simulations. Secondly, numerical simulations are performed to predict ship added resistance and vertical motion responses in short and long waves and the results are verified using the available experimental data. Finally, the non-linearities of added resistance and ship motions with unsteady wave patterns in the time domain are investigated with the increase in wave steepness in both short and long waves. The present systematic study demonstrates that the numerical results have a reasonable agreement with the experimental data and emphasizes the non-linearity in the prediction of the added resistance and the ship motions with the increasing wave steepness in short and long waves.

© 2018 Society of Naval Architects of Korea. Production and hosting by Elsevier B.V. This is an open access article under the CC BY-NC-ND license (<http://creativecommons.org/licenses/by-nc-nd/4.0/>).

1. Introduction

Shipping is the most energy efficient mode of transport and there are many opportunities for an improvement in the energy efficiency and in the associated emissions. Therefore more than ever, advanced ship technologies for the reduction of the ship emissions and maximisation of the energy efficiency are required and sought across the shipping industry. Regarding the ship resistance and propulsion efficiencies, traditionally only the calm water performance is considered at the ship design stage even though recently there have been studies in the optimization of a hull form for a specific range of draught and speed ranges considering the operational profile (Kim and Park, 2015). However, when a ship advances in a seaway, she requires additional power in comparison with the power required in calm water due to weather effects and ship operating conditions. This degradation of the ship performance in a seaway is accounted for by the application of a “Sea Margin” onto the total required engine power. The added resistance

due to waves is one of the major components affecting ship performance in a seaway. Therefore, accurate prediction of the added resistance in waves is essential to evaluate the additional power, to assess environmental impact and to design ships with high fuel efficiency in actual operating conditions with other operation measures, such as voyage planning and weather routing. Also, the correct estimation and understanding of the ship motions are crucial to ensure safe navigation of ships.

Recently there are a number of important developments regarding the environmental regulations driven by the historic Paris Agreement (U.N, 2015) in the climate change and by the International Maritime Organization (IMO). Marine Environment Protection Committee (MEPC) of IMO issued new regulations to improve the energy efficiency level of ships and to reduce carbon emissions. These regulations include the Energy Efficiency Design Index (EEDI) for new ships as a mandatory technical measure and the Ship Energy Efficiency Management Plan (SEEMP) for ships in service to manage ship and fleet efficiency using the Energy Efficiency Operational Indicator (EEOI) as a monitoring tool. Recently, the ship speed reduction coefficient (f_w) has been proposed and is under discussion for the calculation of EEDI in representative sea states (IMO, 2012; ITTC, 2014).

The added resistance in waves can be broken down into three

* Corresponding author.

E-mail address: olgun.hizir@strath.ac.uk (O. Hizir).

Peer review under responsibility of Society of Naval Architects of Korea.

components: the wave radiation originated by the ship motions, the phase shift between the wave excitation and the ship motions, and the diffraction of incident waves by the ship hull. Especially added resistance in short waves is one of the predominant factors for a large ship's performance because most of the time ships travel in relatively short wave length conditions under low sea states hence the added resistance in short waves preserves its importance which means a reliable prediction of the added resistance in short waves is crucial for the accurate estimation of a ship's performance in waves.

In experimental studies, the accurate estimation of the added resistance in short waves is a challenging problem due to the sensitivity of the experimental setup to measure very small quantities and the uncertainties in the measured data (Liu and Papanikolaou, 2016). In numerical simulations, the accurate estimation of the added resistance is difficult in short waves because very dense grids or small size panels are needed to simulate wave patterns accurately while the non-linear hydrodynamic effects are intensified in short waves due to the dominant diffraction component primarily generated near the ship bow. Ley et al. (2014) indicated that viscous effects play an important role in the prediction of the added resistance in short waves. In potential flow methods, added resistance is estimated using the far-field method and the near-field method. The estimation of added resistance using the far-field method was first introduced by Mauro (1960) using the Kochin function which consists of radiating and diffracting wave components. Later on, the far-field method based on the radiated energy approach was proposed by Gerritsma and Beukelman (1972) for added resistance in head seas and has become popular in strip theory programs due to its easy implementation. Recently Liu et al. (2011) solved the added resistance problem using the hybrid Rankine Source-Green function method considering the asymptotic and empirical methods which improved the results in short waves. The near-field method was first introduced by Havelock (1937) and was enhanced by Faltinsen et al. (1980) based on the direct pressure integration approach. Salvesen et al. (1970) introduced a simplified asymptotic method based on 2-D strip theory to overcome the deficiency of this approach in short waves. Kim et al. (2007) and Joncquez (2009) formulated the added resistance based on the Rankine panel method using a time-domain approach with B-spline functions. Seo et al. (2013) predicted the added resistance of KCS and KVLCC2 based on the time-domain Rankine panel method using in weakly-nonlinear and weak-scatterer approaches combining three types of Ax-bow shape. Park et al. (2016) predicted the added resistance of KVLCC2 at different drafts using the frequency-domain strip method and time-domain Rankine panel method. Although recently nonlinear analytical techniques are applied to show nonlinearity in motion and added resistance estimations, in the current study, only linear potential method is used to show the superiority of the CFD for the added resistance estimations compared to potential methods.

As computational facilities have become more powerful and more accessible, CFD tools are now increasingly applied used to predict added resistance and ship motions especially to account for their nonlinearities. Deng et al. (2010), El Moctar et al. (2010) and Sadat-Hosseini et al. (2010) predicted the added resistance of KVLCC2 in head waves using CFD tools as presented at the Gothenburg (2010), SIMMAN (2014) and SHOPERA (2016) Workshops. Guo et al. (2012) investigated the added resistance, ship motions and wake flow of KVLCC2 in head waves with systematic validation and verification of the numerical computation and Sadat-Hosseini et al. (2013) predicted the added resistance and motions for KVLCC2 using the in-house code CFDSHIP-IOWA which

is based on a (Unsteady Reynolds-Averaged Navier–Stokes) URANS approach. In addition to the studies on the prediction of added resistance and ship motions in waves, there have been subsequent investigations on how to reduce the added resistance by modifying the hull form. Park et al. (2014) and Kim et al. (2015) modified the fore body of KVLCC2 to reduce the added resistance in waves and Kim et al. (2014) modified the bulbous bow of a containership to optimize the hull form for both operating conditions in calm water and waves.

In the semi-empirical methods as for a practical approach, Fujii and Takahashi (1975) derived a semi-empirical formula to correct the prediction of the added resistance in short waves by adopting complementary coefficients to drift force formulas and Faltinsen et al. (1980) introduced a simplified asymptotic method to complement the deficiency of this approach in short waves taking into account the interaction of diffraction waves. Recently Liu et al. (2015) proposed a semi-empirical formula in combination with the far-field method to predict the added resistance in short waves. There have also been investigations concerning the increase in the required power and the ship speed loss due to waves. Kwon (2008) predicted the ship speed loss using semi-empirical model considering the wind, motions, and diffraction resistance while Prpić-Oršić and Faltinsen (2012) investigated the ship speed loss and CO₂ emissions considering the added resistance due to waves and the propeller performance in actual sea, and Kim et al. (2017a) presented a reliable methodology to estimate the added resistance and the ship speed loss of a containership due to wind and waves in random seas.

In the present study, added resistance of KVLCC2 with the increasing wave steepness in regular head seas have been studied numerically using URANS method in CFD and using the 3-D linear potential method. The numerical simulations including grid convergence tests for CFD and the 3-D linear potential methods are performed to predict the ship added resistance and vertical motion responses (heave and pitch) in regular waves and results are used for validation with the available experimental data. The added resistance force components in both short and long wave conditions are calculated using 3-D linear potential method to investigate the significance of each component in different wave conditions. Also, time history results of total resistance and ship vertical motions with unsteady wave patterns are simulated and analysed using the CFD method in both short and long wave conditions to investigate the effects of wave radiation and diffraction and nonlinear characteristics such as the water on deck. Finally, the relationship between the added resistance and the ship vertical motions and their nonlinearities are investigated with varying wave steepness for short and long waves.

2. Ship particulars and coordinate system

All calculations of the added resistance and ship motions have been performed for KVLCC2, which represents the second variant of the VLCC-type vessel developed by the Korea Research Institute of Ships and Ocean Engineering (KRISO) which is one of benchmark hull forms used to study seakeeping problems by researchers. The main particulars of the KVLCC2 are given in full scale in Table 1. For CFD simulations, a model scale vessel without appendages using a scale ratio of 1/80 is employed in the calculations.

In the numerical simulations, a right-handed coordinate system x, y, z is adopted. The translational displacements in the x, y and z directions are ξ_1 (surge), ξ_2 (sway) and ξ_3 (heave), and the angular displacements of rotational motion about the x, y and z axes are ξ_4 (roll), ξ_5 (pitch) and ξ_6 (yaw) respectively and θ angle represents the

Table 1
Main particulars of KVLCC2.

Particulars	Full Scale	Model Scale
Length, L (m)	320	4
Breadth, B (m)	58	0.725
Depth, D (m)	30	0.375
Draught, T (m)	20.8	0.260
Displacement, V (m ³)	312,622	0.6106
LCG (%), fwd +	3.48	3.48
VCG (m)	18.56	0.232
Block coefficient, C_B (-)	0.8098	0.8098

ship's heading angle with respect to the incident waves. For head seas the angle θ equals 180° and for beam seas from the port side the angle equals 90°.

3. Numerical methods and modelling

In the present study, the 3-D linear potential flow and CFD methods are applied to predict the added resistance and the vertical ship motions in regular head waves.

3.1. 3-D linear potential method

3-D potential flow calculations are carried out using PRECAL (PREssure CALculation) software developed by Maritime Research Institute Netherlands (MARIN) (Van't Veer, 2009). PRECAL software is based on the planar panel approach which can calculate the seakeeping behaviour of monohull, catamaran and trimaran ships. In addition to the rigid body motions, it can also calculate the deformation modes of a ship's hull girder, internal loads, pressure on the hull and added resistance in waves. The prediction of the forward speed effects is the main shortcoming in the solution of Green's functions due to the complex numerical integration process on the waterline sections. Numerical methods need to be implemented to solve Boundary Value Problem (BVP) in the presence of forward speed and the Green's functions need to be satisfied both for the Free-Surface Boundary Condition (FSBC) and the Body Boundary Condition (BBC). PRECAL is a 3-D source-sink frequency domain code capable of solving the forward speed linear BVP using the Approximate Forward Speed (AFS) and the Exact Forward Speed (EFS) methods. In the AFS method the BVP is solved using zero-speed Green's functions and then forward speed corrections are applied to the BVP equations. It is possible to use the Lid panel method (Lee and Sclavounos, 1989) where waterplane area (Lid) panels are used to suppress the occurrence of the irregular frequencies in the BVP solutions. In the EFS method, exact forward speed Green's functions are used to solve the forward speed BVP, but in PRECAL software Lid panel method can only be applied to the AFS formulation. In this study, forward speed ship motions are solved using the AFS formulation due to its fast and accurate results (Hizir, 2015). In the AFS formulation the BVP is solved using zero-speed Green's functions and the forward speed influence is accounted for the forward speed correction terms appearing in the hydrodynamic pressure, FSBC, BBC equations (Van't Veer, 2009). The added resistance is calculated using the near-field method based on direct pressure integration over the mean wetted hull surface, using the second-order forces to calculate wave drift forces while the first-order forces and moments are calculated to solve the ship motions. The total pressure is divided into four components which originate from the relative water height, incident wave velocities, the pressure gradient and the rotation times inertial terms. The added resistance force due to waves (ΔR_{wave}) is calculated in the time domain as shown in Eq. (1)

$$\Delta R_{wave} = \left[\begin{array}{c} -\rho \int_{H_0} \vec{\nabla} \phi^{(1)} \cdot \vec{\nabla} \phi^{(1)} \vec{n}^{(0)} ds \\ -\rho \int_{H_0} (\vec{\alpha}^{(1)} \cdot \vec{\nabla}) \left(\frac{\partial \phi^{(1)}}{\partial t} + \vec{\nabla} \phi^{(1)} \cdot \vec{\nabla} \bar{\phi} \right) \vec{n}^{(0)} ds \\ + \frac{1}{2} \rho g \int_{wl} (\zeta^{(1)} - \alpha_3^{(1)})^2 \vec{n}^{(0)} dl + \vec{\Omega}^{(1)} \times M \ddot{\bar{X}}^{(1)} \end{array} \right] \quad (1)$$

where the first integral is the water velocity contribution, the second integral is the pressure gradient contribution, the third integral is the relative wave height contribution and the last term is the rotation times inertia contribution. The indices stand for the order of the forces in the force contribution formulations. H_0 represents the mean position of the ship, $\vec{\alpha}^{(1)}$ represents the first order translation and rotation vector, $\vec{n}^{(0)}$ is the zeroth order normal vector calculated on the mean position vessel wetted surface and $\vec{\Omega}^{(1)}$ is the first order rotation vector. In order to derive the added resistance equation in the frequency domain, an oscillatory description of motion and flow is introduced and the steady flow contribution is neglected. The mean added resistance in the frequency domain is formulated by:

$$\Delta R_{wave} = \left[\begin{array}{c} -\rho \int_{H_0} |\vec{\nabla} \phi^{(1)}|^2 \vec{n}^{(0)} ds \\ -\rho \int_{H_0} (\vec{\alpha}^{(1)} \cdot \vec{\nabla}) (i\omega_e \vec{\nabla} \phi^{(1)}) \vec{n}^{(0)} ds \\ + \frac{1}{2} \rho g \int_{wl} |\zeta^{(1)}|^2 \vec{n}^{(0)} dl - \omega_e^2 \vec{\Omega}^{(1)} \times M \bar{X}^{(1)} \end{array} \right] \quad (2)$$

In order to evaluate the added resistance forces, all components in the integrals are defined in perturbation series. A small parameter (ϵ) is introduced to define the quantities in the perturbation series. The perturbation series expansion of the relative wave height and the velocity potential can be formulated as shown in Eqs. (3) and (4):

$$\zeta = \zeta^{(0)} + \epsilon \zeta^{(1)} + \epsilon^2 \zeta^{(2)} + O(\epsilon^3) \quad (3)$$

$$\phi = \bar{\phi} + \epsilon \phi^{(1)} + \epsilon^2 \phi^{(2)} + O(\epsilon^3) \quad (4)$$

where superscripts (0), (1) and (2) denote steady zeroth order, first order and second order quantities. The zeroth order quantities are time independent and are assumed to be small to satisfy the linearized free-surface condition. For the same reason, time dependent parts of the series are also assumed to be small.

Prior to the evaluation of the added resistance, the BVP needs to be solved and the unsteady velocity potential ϕ needs to be calculated. In added resistance calculations, only the mean values of the forces and moments are of interest. First-order quantities such as motions, velocities, accelerations etc. have a mean value of zero when the wave is given by an oscillatory function with a mean value of zero. However, second-order quantities such as added resistance have a non-zero mean value therefore in order to calculate the added resistance, second-order forces and moments need to be calculated. In the present study, in the calculation of added resistance, only the constant part (mean value) of

the added resistance is taken into account while the slowly oscillating part of the added resistance is trivial.

3.2. Computational Fluid Dynamics (CFD)

An URANS approach was applied to calculate the added resistance and ship motions in regular waves using the commercial CFD software STAR-CCM+. For incompressible flows, if there are no external forces, the averaged continuity and momentum equations are given in tensor form in the cartesian coordinate system by Eq. (5) and (6)

$$\frac{\partial(\rho\bar{u}_i)}{\partial x_i} = 0 \tag{5}$$

$$\frac{\partial(\rho\bar{u}_i)}{\partial t} + \frac{\partial}{\partial x_j} \left(\rho\bar{u}_i\bar{u}_j + \rho\overline{u'_i u'_j} \right) = -\frac{\partial\bar{p}}{\partial x_i} + \frac{\partial\bar{\tau}_{ij}}{\partial x_j} \tag{6}$$

where \bar{u}_i is the averaged velocity vector of flow, $\overline{u'_i u'_j}$ is the Reynolds stresses and \bar{p} is the mean pressure. For Newtonian fluid under incompressible flow, the mean shear stress tensor, $\bar{\tau}_{ij}$, is expressed as Eq. (7)

$$\bar{\tau}_{ij} = \mu \left(\frac{\partial\bar{u}_i}{\partial x_j} + \frac{\partial\bar{u}_j}{\partial x_i} \right) \tag{7}$$

where μ is dynamic viscosity.

The Finite Volume Method (FVM) and the Volume of Fluid (VOF) method were applied to the spatial discretization and free surface capturing respectively. The flow equations were solved in a segregated manner using a predictor-corrector approach. Convection and diffusion terms in the RANS equations were discretised by a second-order upwind scheme and a central difference scheme. The semi-implicit method for pressure-linked equations (SIMPLE) algorithm was used to resolve the pressure-velocity coupling and a standard $k - \epsilon$ model was applied as the turbulence model. In order to consider ship motions, a Dynamic Fluid Body Interaction (DFBI) scheme was applied with the vessel free to move in heave and pitch directions as vertical motions.

Only half of the ship's hull (the port side) with a scale ratio of 1/80 and control volume were taken into account in the calculations, thus a symmetry plane formed the centreline domain face in order to reduce computational time and complexity. The calculation domain is $-3L < x < \lambda$, $0 < y < 2L$, $-2L < z < 1L$ where the mid-plane of the ship is located at $y = 0$, ship draught (T) is at $z = 0$ and λ is

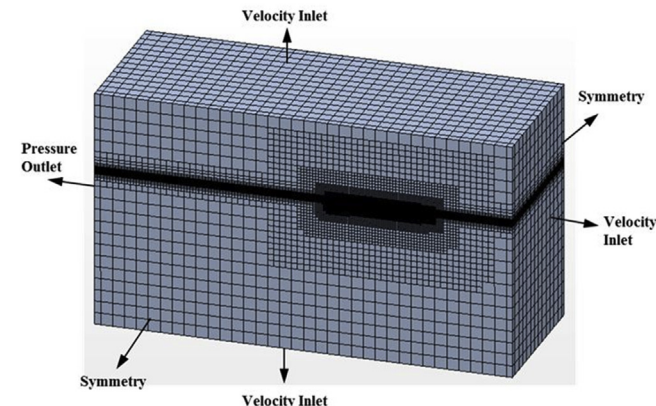


Fig. 1. Mesh and boundary conditions.

the wave length assumed to be $\lambda = gT^2/2\pi$ for deep water. The boundary conditions together with the generated meshes are depicted in Fig. 1. Artificial wave damping was applied to avoid the undesirable effect of the reflected waves from the side and outlet boundaries. As shown in Fig. 1, near the free surface and around the hull local mesh refinements were applied to resolve the wave-pattern and the incident wave field.

4. Discussion of results

The simulation results using CFD and 3-D potential methods are presented and compared with available experimental added resistance and ship motions data in regular head waves. Unsteady wave patterns and time history results of the resistance and ship motions in waves are simulated using a CFD method. Only two degrees of freedom motions, which are heave and pitch responses, are calculated during all simulations. All simulations are carried out at the design ship speed of 15.5 knots, which corresponds to a Froude Number (Fn) of 0.142 and a Reynolds Number (Rn) of $3.82E+6$ for CFD.

4.1. Grid convergence test

Prior to the investigation of the added resistance and the heave and pitch motions using the CFD tool, grid convergence tests were performed to capture the accurate wave length and height on the free surface for not only long wave ($\lambda/L = 1.2$), but also for short ($\lambda/L = 0.5$) wave conditions because in short waves when coarse mesh is used the added resistance might be underestimated. Ley et al. (2014) and Seo et al. (2014) indicated that the added resistance of KVLCC2 is quite sensitive to the grid spacing near the bow region. The wave steepness (H/λ) is taken as 1/60 and long wave condition corresponds to a resonant case (Sadat-Hosseini et al. (2013)). The coarse and fine mesh systems are derived by reducing and increasing cell numbers per wave length and cell height on free surface respectively using a factor of $\sqrt{2}$ (Böckmann et al., 2014) based on the base mesh case (Case no. C11 and C14 for short and long wave conditions in Table 2). The simulation time step is set to be proportional to the grid size as shown in Table 2 where T_e represents the corresponding encountering period.

The results of the convergence tests with three different mesh systems in short and long waves are shown in Fig. 2 where ρ , g and A denote the density, gravitational acceleration, and the wave amplitude parameters respectively. As the number of cells increased, the added resistance coefficient increased, especially from the coarse mesh to base mesh system for short wave case. The test results of the added resistance for the base and fine mesh show a monotonic convergence with the convergence ratio (R_C) of 0.462 and 0.478 in short and long waves respectively (Stern et al., 2006), which indicates that the effects of the grid change are accepted to be small between base and fine mesh system (Tezdogan et al., 2015). The grid uncertainty analysis using grid triplets G1, G2 and G3 with a uniform parameter ratio (r_G) chosen to be $\sqrt{2}$ for the free surface refinement, which shows the grid uncertainty (U_G) for the base mesh with 3.337% S_2 and 3.759% S_2 in short (Case no. C11) and long (Case no. C14) waves respectively based on the Grid

Table 2
Test cases for grid convergence ($\lambda/L = 0.5$ and 1.2, $H/\lambda = 1/60$).

Case no.	Mesh	$\lambda/\Delta x$	$H/\Delta z$	$T_e/\Delta t$
C11C/C14C	Coarse(C)	70	14	181
C11/C14	Base	100	20	256 (2 ⁸)
C11F/C14F	Fine(F)	140	28	362

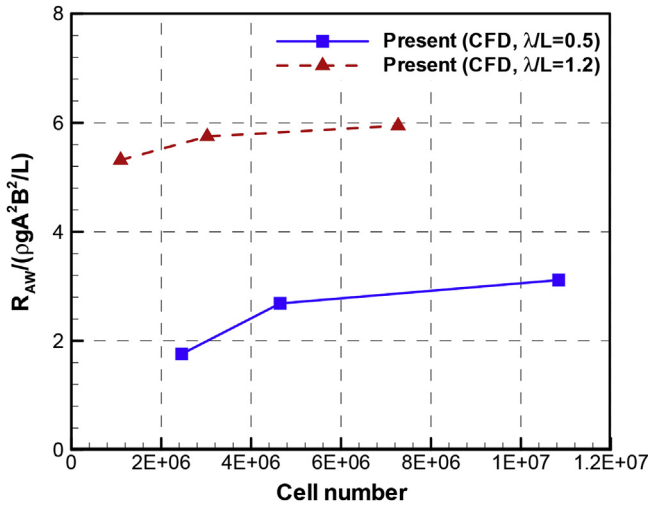


Fig. 2. Grid convergence test for the added resistance in short ($\lambda/L=0.5$) and long ($\lambda/L=1.2$) waves.

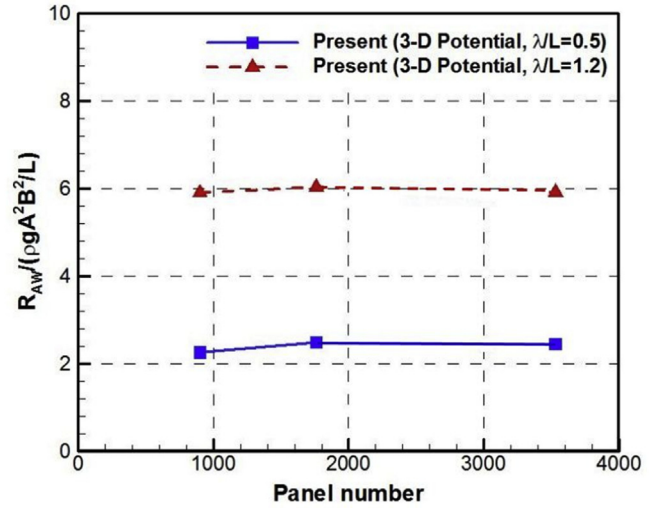


Fig. 3. Panel number convergence test for the added resistance in short ($\lambda/L=0.5$) and long ($\lambda/L=1.2$) waves.

Convergence Index (GCI) method, where S_1 , S_2 and S_3 are corresponding to the solutions with fine, base and coarse meshes. Additionally the time-step convergence study was conducted and shows that the time-step uncertainty (U_T) results for the base mesh are $0.794\%S_2$ and $0.872\%S_2$ in short and long waves respectively based on GCI method. In both grid and time-step convergence study, reasonable small levels of uncertainty were estimated. For more detailed information on the calculation of the uncertainty analysis, reference can be made to Stern et al. (2006). Therefore, the base mesh system was chosen for the CFD simulations in this study for both short and long wave cases and the cell number and time step vary according to the wave conditions in the simulations. Fig. 2 also demonstrates that in short waves higher number of cells are needed to satisfy the convergence hence simulations in short waves are computationally more expensive relatively to the simulations in long waves.

Prior to the 3-D potential flow method calculations, added resistance convergence tests are performed to capture minimum required panel number which converges the added resistance of KVLCC2. In all simulations, panel numbers represent the half of the discretised ship's hull under the still water level. In the added resistance convergence tests, vessel's hull is discretised by a coarse, base and fine mesh variations. The coarse and fine mesh systems are derived by reducing and increasing the total panel numbers on the vessel's surface under still water level using a factor of 2 based on the base mesh which is modelled using 1760 quadratic and triangular panels. In all mesh variations minimum 8 panels per wave length as the maximum length of each panel are used for the highest encounter frequency. The results of the added resistance convergence tests with the varying total panel number are shown in Table 3 and Fig. 3.

Likewise the CFD grid convergence results, it can be seen from Fig. 3 when the number of panels are increased, the added

resistance coefficient are increased, especially from the coarse mesh to base mesh system for short wave case. Also uncertainty analysis for mean added resistance results obtained from potential method was carried out, which shows oscillatory convergence with the convergence ratio (R_C) of -0.168 and -0.765 in short and long waves respectively, and the grid uncertainty (U_G) for the base mesh with $3.313\%S_2$ and $5.615\%S_2$ in short and long waves based on the GCI method. Therefore, in the following 3-D flow method calculations the base mesh system is used.

The average added resistance due to waves ($\overline{R_{AW}}$) is obtained by Eq. (8)

$$\overline{R_{AW}} = R_w - R_c \tag{8}$$

where R_w and R_c are total resistance in waves and resistance in calm water respectively.

Fig. 4 shows the results of the time history of the ship total resistance in short and long waves which are oscillating periodically with corresponding encounter periods (i.e. $T_e = 0.7525$ and 1.3227 s for short and long waves respectively) as shown in Table 4.

4.2. Added resistance and ship motions

Following the CFD grid convergence tests, numerical calculations using the 3-D potential and CFD methods at the ship speed of 15.5 knots were carried out in both calm water and wave conditions for various wave lengths for constant wave steepness (H/λ) ratio of $1/60$. The test cases are summarised in Table 4.

Prior to the investigation on the added resistance, Response Amplitude Operators (RAOs) of heave and pitch motions are compared with the experimental data in regular head waves from Osaka University (Larsson et al., 2010) and Lee et al. (2013) as shown in Fig. 5. It is a well-known fact that the added resistance is proportional to the relative motions, hence heave and pitch motions, and inaccuracies in the predicted motion responses may amplify the errors in the added resistance calculations. In this study, ξ_3 and ξ_5 are the amplitudes of heave and pitch motion responses respectively whereas $k = 2\pi/\lambda$ is the wave number in deep water. The motion responses are evaluated at the ship's centre of gravity. The zeroth and first order terms of the resistance and motion responses calculated by CFD are used for the added resistance coefficient and motion transfer functions (Shen and Wan,

Table 3
Test cases for grid convergence ($\lambda/L=0.5$ and 1.2 , $A=1m$).

Mesh	Total Panel Number	Added Resistance Coefficient			
		$\lambda/L=0.5$	Difference %	$\lambda/L=1.2$	Difference%
Coarse	900	2.257	-8.0%	5.906	-2.2%
Base	1760	2.457	0.0%	6.038	0.0%
Fine	3560	2.421	-1.3%	5.937	-1.7%

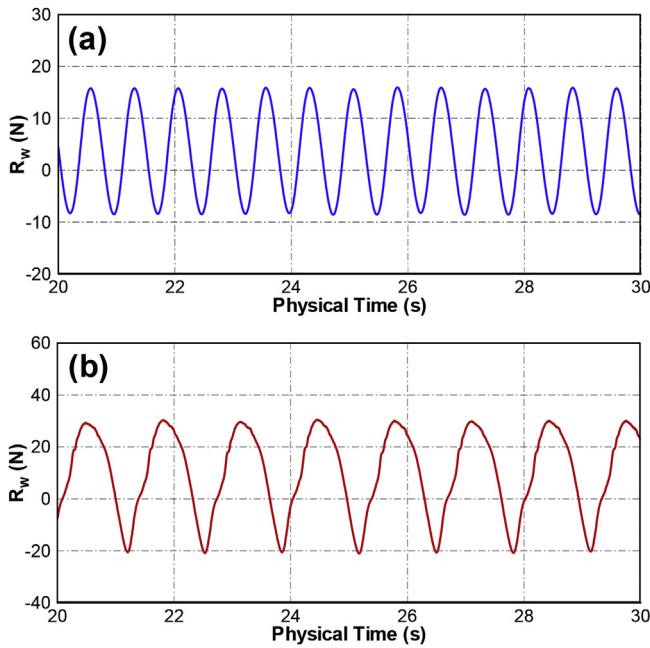


Fig. 4. Time histories of total resistance in (a) short ($\lambda/L = 0.5$) and (b) long ($\lambda/L = 1.2$) waves.

2013). The overestimation of the heave motion using the 3-D potential method is amplified around the resonance period ($1.0 < \lambda/L < 1.4$), while CFD method slightly underestimates the heave motion around the resonance period for the range of λ/L from 1 to 1.4. For the pitch motions, the results obtained from both methods show good agreement with the experimental data. The overestimation of the results obtained from the 3-D potential method for the heave motions can be attributed to the AFS formulation, in which the BVP is solved using zero speed Green's functions and then forward speed corrections are applied to the boundary conditions, and also to Neumann-Kelvin (NK) approximation where the steady wave and unsteady wave interactions are linearized. Kim and Shin (2007) presented a study about the steady and unsteady flow interaction effects on advancing ships and showed that in heave and pitch responses the NK approach overestimates the heave and pitch responses compared to the experimental results. The underestimation of the results obtained from the CFD method is likely to stem from the adoption of a non-inertial reference frame in which large amplitude motion causes inaccurate capturing of the free surface.

The numerical results of the added resistance are compared with the available experiment data (Lee et al., 2013; Sadat-Hosseini et al., 2013) as presented in Fig. 6, which indicates that the CFD and 3-D panel methods both have reasonable agreement with the

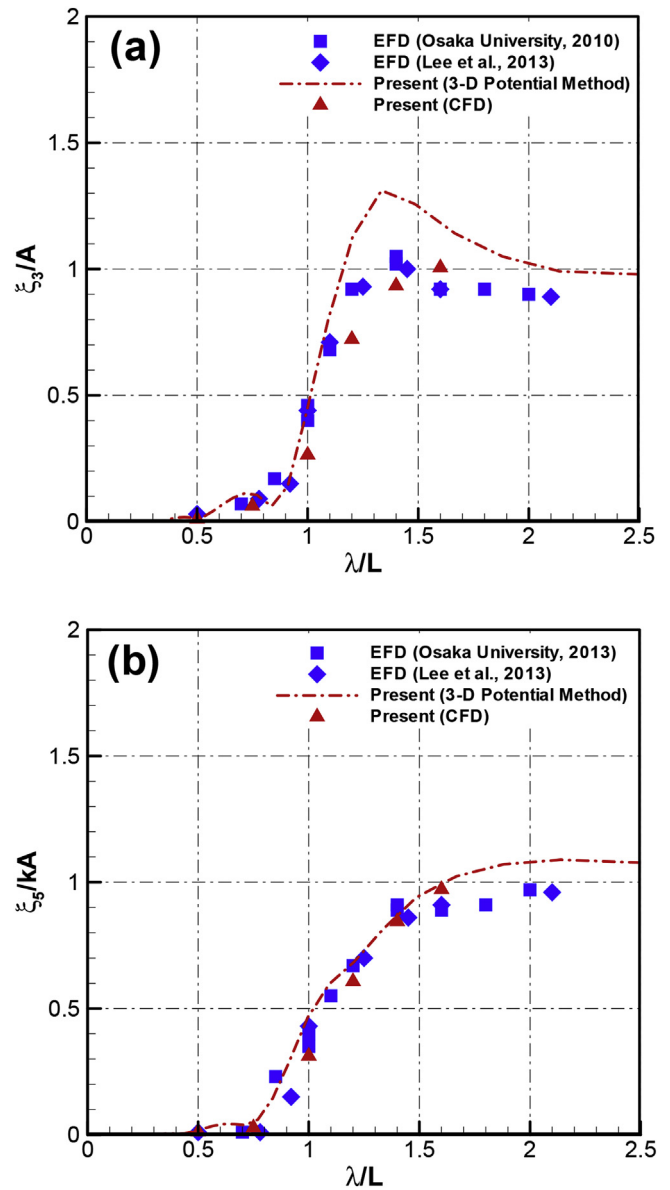


Fig. 5. Response Amplitude Operators (RAOs) for (a) heave and (b) pitch ($V_s = 15.5$ knots, $\theta = 180^\circ$).

experimental data. At $\lambda/L = 0.3$ in short waves, 3-D potential method underestimates the added resistance compared to the experimental and the CFD results. This is due to the panel size around the bow region where the longest side of panels needs to be smaller than $1/7$ of the corresponding wave length. It is observed

Table 4
Test cases at design speed (15.5 knots).

Case no.	V_s [knots]	Wave length (λ/L)	Wave height (H) [m]	Wave steepness (H/ λ)	ω_e [rad/s] (model)	T_e [sec.] (model)
C00	15.5	Calm water	–	–	–	–
C10		0.30	1.60	1/60	11.835	0.5309
C11		0.50	2.67		8.3522	0.7523
C12		0.75	4.00		6.4000	0.9818
C13		1.00	5.33		5.3256	1.1798
C14		1.20	6.40		4.7500	1.3227
C15		1.40	7.47		4.3178	1.4552
C16		1.60	8.53		3.9785	1.5793

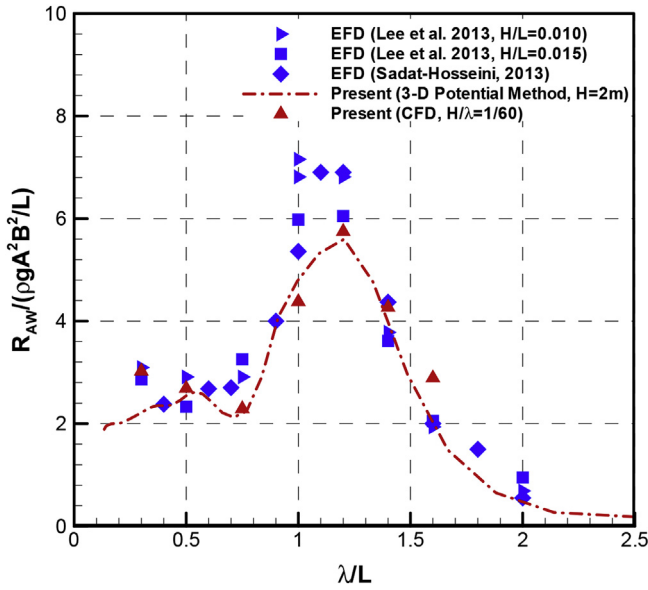


Fig. 6. Added resistance ($V_s = 15.5$ knots, $\theta = 180^\circ$).

that experimental results from Lee et al. (2013) show the difference of the added resistance for wave steepness between $H/L = 0.010$ and $H/L = 0.015$ especially in long waves ($1.0 < \lambda/L < 1.2$), which will be discussed later in this paper.

The time histories of total resistance force and non-dimensional heave and pitch motions for short ($\lambda/L = 0.5$) and long ($\lambda/L = 1.2$) waves are displayed over an encounter period as shown in Fig. 7. The largest resistance force in waves is observed around $t/Te = 0.5$. Fig. 7 shows that in long waves the added resistance is dominantly affected by wave radiation due to the ship motions, while in short waves the added resistance is dominantly affected by the diffraction of incident waves primarily due to the ship bow hull as presented in Fig. 8(b) whereas the ship motions are almost negligible. Despite the oscillation amplitudes of the vertical ship motions are almost zero in short waves as shown in Fig. 7(b) and (c) and there is no significant phenomena of green water on deck as presented in Fig. 8(c) and (d), the amplitude of the total resistance in time domain is seen to be relatively high compared to those in long waves due to the wave diffraction near the ship bow. In the current study, 1st order motion and added resistance response signals appears as prominent compared to 2nd order responses, especially in the case of $\lambda/L = 0.5$. This can be explained as the lack of geometrical non-linearity of tanker hulls which have long vertical walls and this results in small non-linearity in vessel motion responses and hence in relative motions and the added resistance of the tankers. As it can be observed from Fig. 7, even though the wave slope is constant, the total resistance of the tanker is sinusoidal for the case of $\lambda/L = 0.5$. The 2nd order responses can be observed in the $\lambda/L = 1.2$ case, which is mainly due to the augmented motion responses around the peak period.

Similarly to Fig. 7, the ship motions and wave patterns in short and long wave conditions are captured and visualized in Fig. 8 at $t/Te = 0.0$ and $t/Te = 0.5$ when the ship has the smallest and largest resistance value respectively. Fig. 8(a) illustrates that in long waves the bow is completely immersed with green water on deck mostly due to heave motion, while the pitch amplitude is almost zero as shown in Fig. 7(c). It is observed that in Fig. 8(a) and (b) for long wave conditions there are significant differences in wave patterns such as bow immersion and ship motions show especially heave

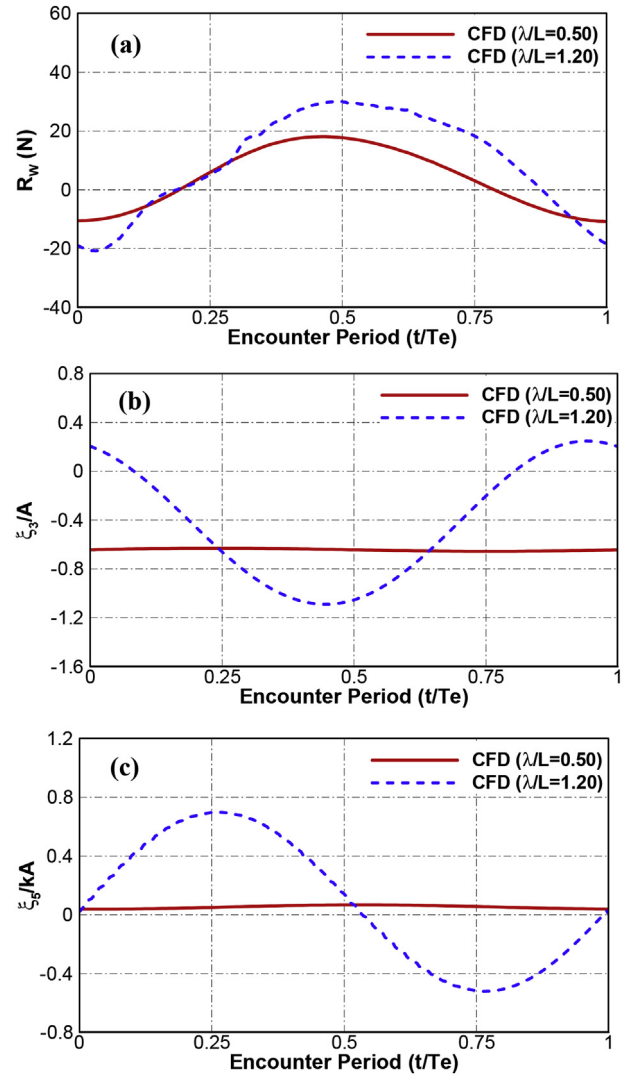


Fig. 7. Time histories of (a) total resistance, and non-dimensional (b) heave and (c) pitch responses at a period of encounter in short and long wave conditions.

motion as shown Fig. 7(b). On the other hand, in Fig. 8(c) and (d) for short wave simulations there is no significant difference except diffracted waves mainly generated near the ship bow and wave elevations, which indicates that the diffraction wave near the bow region is the predominant component of the added resistance whereas the oscillation amplitudes of the vertical ship motions are almost negligible compared to those in long waves as shown in Fig. 7(b) and (c) and presented in Fig. 8(c) and (d). Moreover, the influence of the pressure components in Eq. (2) to the total added resistance is investigated using 3-D potential flow method at the vessel design speed for the $\lambda/L = 0.5$ and 1.2 conditions. The results influence of the pressure components to the added resistance is summarised in Table 5.

It can be observed in Table 5 that the maximum contribution to the added resistance is from the relative wave height component in Eq. (2) for both at $\lambda/L = 0.5$ and 1.2 conditions. Furthermore, the relative wave height and the water velocity terms of the added resistance forces for the short wave simulation is observed to be quarter and half of the estimated long wave simulation results respectively. In short wave simulations, the pressure gradient and

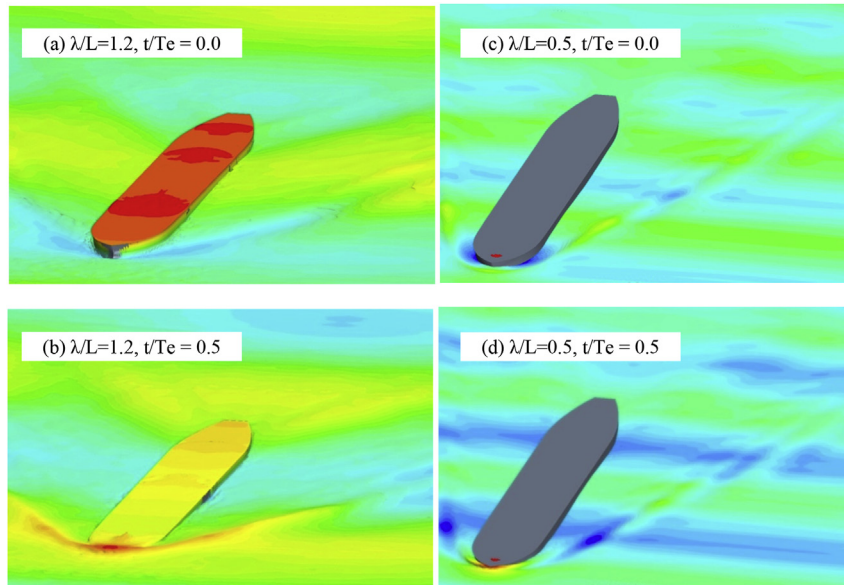


Fig. 8. Illustration of free surface elevation at (a) $\lambda/L = 1.2$ at $t/Te = 0.0$, (b) at $t/Te = 0.5$ and at (c) $\lambda/L = 0.5$ at $t/Te = 0.0$, (d) at $t/Te = 0.5$.

Table 5
Non-dimensional mean added resistance components at design speed (15.5 knots) at $\lambda/L = 0.5$ and 1.2

Added Resistance Components	Non-dimensional Mean Added Resistance ($R_{aw}/(\rho g A^2 B^2/L)$)	
	$\lambda/L = 0.5$	$\lambda/L = 1.2$
Relative wave height	-4.250	-17.956
Water velocity	1.696	3.618
Pressure gradient	0.083	6.815
Rotation*Inertia	-0.013	1.485
Total	-2.484	-6.038

rotation times inertia terms are small compared to the long wave simulations. Blok (1993) investigated the sign convention and the contribution of the added resistance components in numerical calculations. The author observed that the added resistance forces are mainly applied at the bow section. The relative wave height term has the largest contribution and invariably it has a negative sign, hence it increases the added resistance force. The water velocity term represents the kinetic term in the Bernoulli equation which brings about a suction force at the bow higher than the stern due to larger water velocity disturbances at the bow than at the stern. The rotation times inertia term can be positive or negative and when in phase they contribute to a suction force which is larger at the bow than at the stern. The pressure gradient depends on the coupling between the heave and pitch motions. At the pitch resonance, when the bow is in submerged position, the position of the centre of gravity is being accelerated upward which produces an upward fluid force component contributes in the propulsive force.

4.3. Added resistance and ship motions with varying wave steepness

The relationship between the added resistance and the ship vertical motions for the wave steepness (H/λ) are investigated for short ($\lambda/L = 0.5$) and long ($\lambda/L = 1.2$) wave conditions at the ship speed of 15.5knots as summarised in Table 6.

Fig. 9 presents the results of the first order harmonic amplitudes of the vertical ship motions in long waves with varying wave steepness obtained from the CFD analysis, and the comparison of

these results with those obtained from the 3-D panel code. It was indicated by Kim et al. (2017b) that the vertical motions calculated using CFD, especially the non-dimensional heave motions, decrease non-linearly with the increase in wave steepness (H/λ).

In Fig. 10 the results of the added resistance obtained from the CFD are compared with the 3-D potential results. Fig. 10(a) indicates that the increase in the added resistance is related quadratically to the increase in the wave height. The 3-D potential results are almost identical to the quadratic interpolation curve, while CFD results have lower values than the quadratic curve as the wave steepness increases due to the increase of the non-linearity. The added resistance coefficient is presented in Fig. 10(b) which shows the non-linear behaviour of added resistance with the increasing wave steepness. It is also observed in Fig. 10(b) that the added resistance coefficient in long waves is decreasing with the increase in wave steepness, which could explain the decrease of added resistance coefficient for experimental results from Lee et al. (2013) in long waves ($1.0 < \lambda/L < 1.2$) as shown in Fig. 6.

On the other hand, in short waves, the first order harmonic amplitudes of the non-dimensional heave and pitch motions with varying wave steepness obtained from both the CFD and the 3-D potential flow methods stayed almost constant with the increase in wave steepness as shown in Fig. 11(a) and Fig. 11(b).

Fig. 12(a) shows that the magnitudes of the added resistance in short waves are much smaller than those in long waves as shown in Fig. 10(a), which indicates that the added resistance in short waves is difficult to predict experimentally and numerically (Seo et al., 2014). Fig. 12(b) presents that the added resistance coefficient in short waves is decreasing with the increase in the wave steepness. The order of the decrement of the added resistance coefficient with the increase in the wave steepness is smaller in the short waves compared to the long waves. In numbers, the decrement ratio of the added resistance coefficient for wave steepness (H/λ) can be given as for the short waves around 16% whilst the decrement ratio for the long waves is around 67% from the lowest to the highest wave steepness in short and long wave conditions.

5. Conclusions

The added resistance and the vertical ship motions (heave and

Table 6
Test cases for wave steepness at $V_s = 15.5$ knots.

Case no.	Wave length (λ/L)	Wave steepness (H/λ)	Wave height (H) [m]	ω_e [rad/s] (model)	T_e [sec.] (model)
C110	0.5	1/60	2.67	8.3522	0.7523
C111		1/50	3.20		
C112		1/40	4.00		
C113		1/30	5.33		
C140	1.2	1/150	2.56	4.750	1.3227
C141		1/100	3.86		
C142		1/80	4.80		
C143		1/60	6.40		
C144		1/50	7.68		

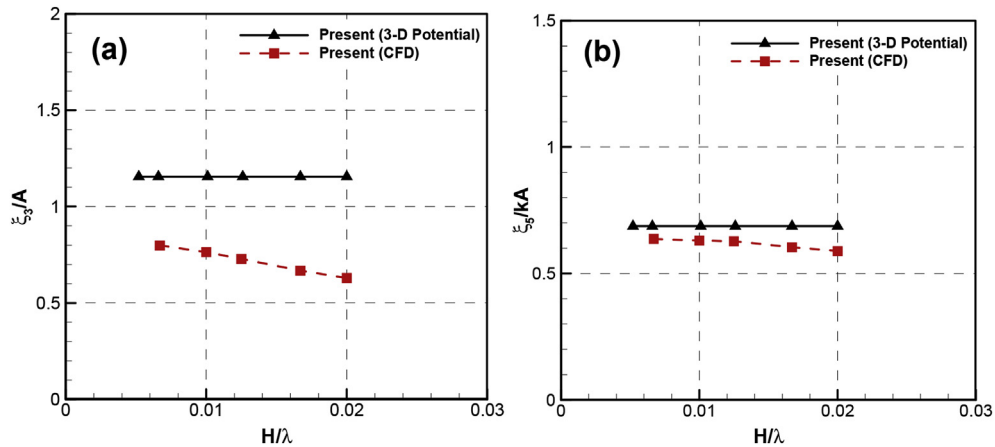


Fig. 9. 1st order harmonic terms of non-dimensional (a) heave and (b) pitch responses in for different wave steepness values ($V_s = 15.5$ knots, $\lambda/L = 1.2$).

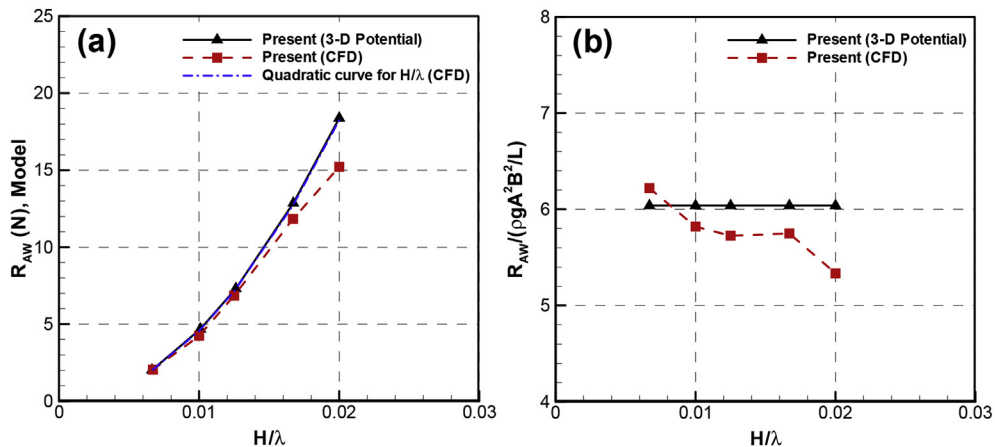


Fig. 10. (a) Added resistance with varying wave steepness at model scale (b) added resistance coefficient with varying wave steepness ($V_s = 15.5$ knots, $\lambda/L = 1.2$).

pitch) of KVLCC2 in regular short and long waves were simulated using the URANS CFD and the 3-D potential flow methods for a wide range of wave conditions at the ship speed of 15.5 knots. The time histories of the total resistance and the ship motions in waves were obtained using the CFD method taking into account the unsteady wave patterns and non-linear effects such as water on deck. The resistance force and the ship motions were investigated with varying wave steepness in short and long wave conditions.

Firstly for the CFD simulations, the optimal mesh system was investigated and established to capture the accurate wave length and height on the free surface from the grid convergence tests on the added resistance in both short and long waves. Also as it was

expected, it was observed that the resistance and the ship motions in waves in the time domain by CFD oscillate periodically at the encounter period for each test conditions.

Secondly the results of the added resistance and the ship motions in regular head waves using the CFD and 3-D potential methods were compared with the available experiment results and they were found to be in a reasonable agreement except for the heave motions which were overestimated by 3-D potential method around the resonance period ($1.0 < \lambda/L < 1.4$) and in long waves ($\lambda/L > 2$) due to the AFS formulation. The heave motions were slightly underestimated by the CFD method for the range of wave lengths (λ/L) from 1 to 1.4 because of the adoption of the non-inertial

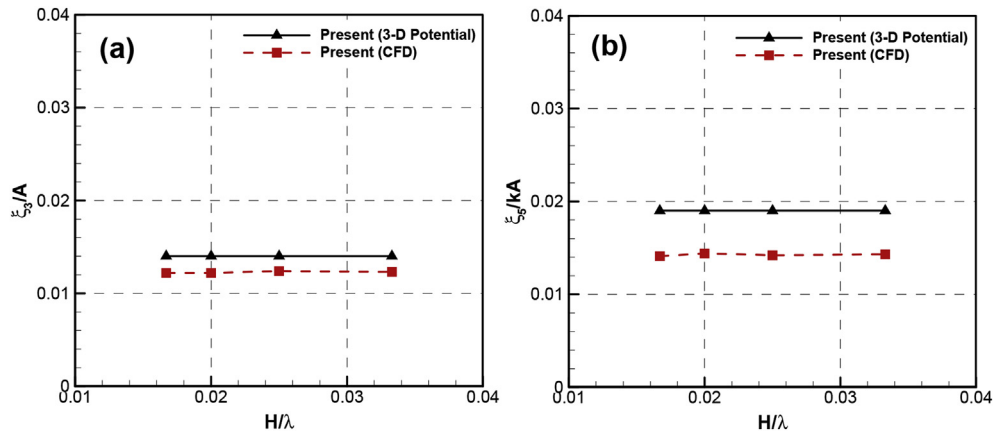


Fig. 11. 1st order harmonic terms of non-dimensional (a) heave and (b) pitch responses for different wave steepness values ($V_s = 15.5$ knots, $\lambda/L = 0.5$).

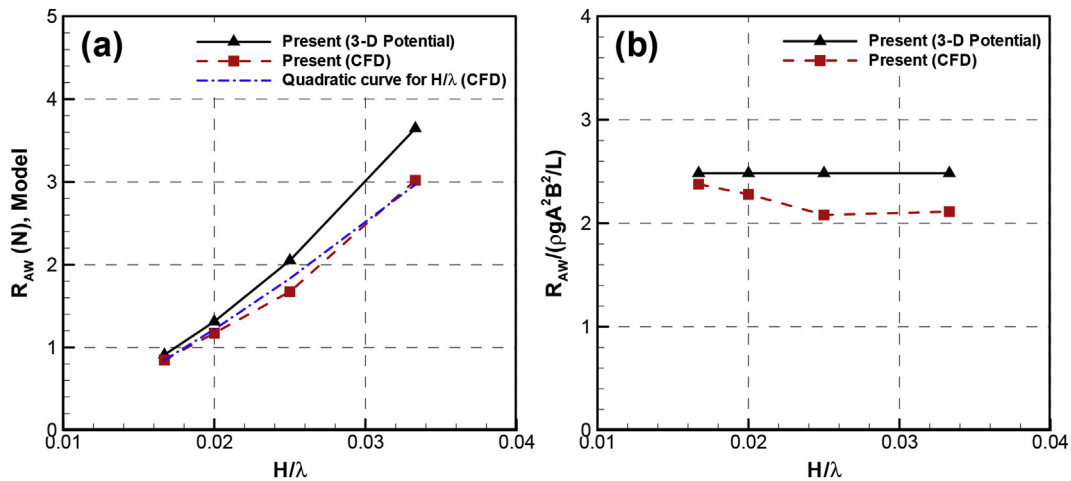


Fig. 12. (a) Added resistance with varying wave steepness at model scale (b) added resistance coefficient with varying wave steepness ($V_s = 15.5$ knots, $\lambda/L = 0.5$).

reference frame. These differences around the resonant period will be investigated in future studies.

Thirdly the time histories of total resistance and ship vertical motions in short ($\lambda/L = 0.5$) and long ($\lambda/L = 1.2$) wave conditions over an encounter period were investigated and compared. Moreover, the influence of the pressure components in the to the total added resistance is investigated using 3-D potential flow method at the vessel design speed for the $\lambda/L = 0.5$ and 1.2 conditions. It was observed that the relative wave height and the water velocity terms of the added resistance forces for the short wave simulation is observed to be quarter and half of the estimated long wave simulation results respectively. In short wave simulations, the pressure gradient and rotation times inertia terms are small compared to the long wave simulations. Also, wave patterns in short and long wave conditions were presented for absolute maximum and minimum values of the added resistance. The water on deck occurrence and the bow immersion was successfully captured in long wave conditions by the current CFD model while in short waves it is observed that the diffracted waves were predominantly generated near the ship.

Finally, the non-linearity of the added resistance and the ship vertical motions were investigated with the varying wave steepness for short ($\lambda/L = 0.5$) and long ($\lambda/L = 1.2$) wave conditions. It was observed that in long waves the vertical motions, especially the

non-dimensional heave motions, decrease non-linearly with the increase in wave steepness while the increase of the added resistance obtained from both the CFD and the 3-D potential methods were observed to be approximately proportional to the square of the wave height. The results of the added resistance using the CFD estimated slightly lower values than those using the 3-D potential method and the added resistance coefficient decreased with the increase in wave steepness. This is due to the increase in the non-linearity as wave steepness increases, which is well captured by the current CFD model. In short waves the vertical ship motions obtained the CFD and the 3-D potential flow methods stayed almost constant with the increase in wave steepness and the increase of the added resistance using CFD in short waves is related quadratically to the wave height whereas the motion amplitudes were much smaller than those in long waves, which means that ship motions are almost negligible in short waves. It is emphasised that the non-linearity of the added resistance and ship motions around the resonance period is larger than in short waves.

Acknowledgements

The authors are grateful to the Engineering and Physical Research Council (EPSRC) for funding the research reported in this paper through the project: “Shipping in Changing Climate. (EPSRC

grant no. EP/K039253/1).

The results given in the paper were obtained using the EPSRC funded ARCHIE-WeSt High Performance Computer (www.archie-west.ac.uk). EPSRC grant no. EP/K000586/1.

References

- Blok, J.J., 1993. The Resistance Increase of a Ship in Waves. Delft University of Technology, TU Delft.
- Böckmann, A., Pákozdi, C., Kristiansen, T., Jang, H., Kim, J., 2014. An experimental and computational development of a benchmark solution for the validation of numerical wave tanks. In: 33rd International Conference on Ocean, Offshore and Arctic Engineering. ASME.
- Deng, G., Leroyer, A., Guilmineau, E., Queutey, P., Visonneau, M., Wackers, J., 2010. Verification and validation for unsteady computation. In: Proceedings of Gothenburg 2010: a Workshop on CFD in Ship Hydrodynamics. Gothenburg, Sweden).
- El Moctar, B., Kaufmann, J., Ley, J., Oberhagemann, J., Shigunov, V., Zorn, T., 2010. Prediction of ship resistance and ship motions using RANSE. In: Proceedings of the Workshop on Numer, p. 1. Ship Hydrodyn., Gothenburg.
- Faltinsen, O.M., Minsaas, K.J., Liapis, N., Skjördal, S.O., 1980. Prediction of resistance and propulsion of a ship in a seaway. In: Proceeding of 13th Symposium on Naval Hydrodynamics, pp. 505–529. Tokyo.
- Fujii, H., Takahashi, T., 1975. Experimental study on the resistance increase of a ship in regular oblique waves. Proceedings of the 14th ITTC 4, 351–360.
- Gerritsma, J., Beukelman, W., 1972. Analysis of the resistance increase in waves of a fast cargo ship. Int. Shipbuild. Prog. 19 (217).
- Gothenburg, 2010. A Workshop on Numerical Ship Hydrodynamics. Denmark.
- Guo, B., Steen, S., Deng, G., 2012. Seakeeping prediction of KVLCC2 in head waves with RANS. Appl. Ocean Res. 35, 56–67.
- Havelock, T.H., 1937. The resistance of a ship among waves. In: Proceedings of the Royal Society of London. Series a, Mathematical and Physical Sciences, pp. 299–308.
- Hizir, O.G., 2015. Three dimensional time domain simulation of ship motions and loads in large amplitude waves. PhD Thesis. Department of Naval Architecture, Ocean and Marine Engineering, pp. 1–240 (University of Strathclyde, Glasgow, UK).
- IMO, 2012. Interim Guidelines for the Calculation of the Coefficient Fw for Decrease in Ship Speed in a Representative Sea Condition for Trial Use. International Maritime Organisation (IMO), London.
- ITTC, 2014. The Specialist Committee on Seakeeping-final Report and Recommendations to the 27th ITTC. International Towing Tank Conference, Copenhagen.
- Jonque, S.A., 2009. Second-order Forces and Moments Acting on Ships in Waves. Technical University of Denmark, Copenhagen, Denmark.
- Kim, B., Shin, Y.S., 2007. Steady flow approximations in three-dimensional ship motion calculation. J. Ship Res. 51 (3), 229–249.
- Kim, H.T., Kim, J.J., Choi, N.Y., Lee, G.H., 2014. A study on the Operating Trim, Shallow Water and Wave Effect. SNAK, pp. 631–637.
- Kim, K.H., Kim, Y., Kim, Y., 2007. WISH JIP Project Report and Manual. Marine Hydrodynamic Laboratory. Seoul National University.
- Kim, M., Hizir, O., Turan, O., Day, S., Incecik, A., 2017a. Estimation of added resistance and ship speed loss in a seaway. Ocean Eng. 141, 465–476.
- Kim, M., Hizir, O., Turan, O., Incecik, A., 2017b. Numerical studies on added resistance and motions of KVLCC2 in head seas for various ship speeds. Ocean Eng. 141, 465–476.
- Kim, M., Park, D.W., 2015. A study on the green ship design for ultra large container ship. J. Kor. Soc. Mar. Environ. Safety 21 (5), 558–570.
- Kim, Y.C., Kim, K.S., Kim, J., Kim, Y.S., Van, S.H., Jang, Y.H., 2015. Calculation of added resistance in waves for KVLCC2 and its modified hull form using RANS-based method, the 25th International Offshore and Polar Engineering Conference. Int. Soc. Offshore and Polar Eng 924–930. Hawaii, USA.
- Kwon, Y.J., 2008. Speed loss due to added resistance in wind and waves. Nav. Archit. 14–16.
- Larsson, L., Stern, F., Visonneau, M., 2010. In: Technology, C.U.o. (Ed.), Proceedings Gothenburg 2010 a Workshop on Numerical Ship Hydrodynamics (Gothenburg, Sweden).
- Lee, C.H., Sclavounos, P.D., 1989. Removing the irregular frequencies from integral equations in wave-body interactions. J. Fluid Mech. 207, 393–418.
- Lee, J.H., Seo, M.G., Park, D.M., Yang, K.K., Kim, K.H., Kim, Y., 2013. Study on the effects of hull form on added resistance. In: The 12th International Symposium on Practical Design of Ships and Other Floating Structures, Changwon, Korea, pp. 329–337.
- Ley, J., Sigmund, S., el Moctar, O., 2014. Numerical prediction of the added resistance of ships in waves. In: 33rd International Conference on Ocean, Offshore and Arctic Engineering. ASME.
- Liu, S., Papanikolaou, A., 2016. Prediction of the Added Resistance of Ships in Oblique Seas. ISOPE.
- Liu, S., Papanikolaou, A., Zaraphonitis, G., 2011. Prediction of added resistance of ships in waves. Ocean Eng. 38 (4), 641–650.
- Liu, S., Papanikolaou, A., Zaraphonitis, G., 2015. Practical approach to the added resistance of a ship in short waves, the twenty-fifth international offshore and polar engineering conference. Int. Soc. Offshore and Polar Eng 11–18.
- Mauro, H., 1960. The drift of a body floating on waves. J. Ship Res. 4, 1–5.
- Park, D.-M., Kim, Y., Seo, M.-G., Lee, J., 2016. Study on added resistance of a tanker in head waves at different drafts. Ocean Eng. 111, 569–581.
- Park, D.M., Seo, M.G., Lee, J., Yang, K.Y., Kim, Y., 2014. Systematic experimental and numerical analyses on added resistance in waves. J. Soc. Naval Arch. Korea 51 (6), 459–479.
- Prpić-Orišić, J., Faltinsen, O.M., 2012. Estimation of ship speed loss and associated CO₂ emissions in a seaway. Ocean Eng. 44, 1–10.
- Sadat-Hosseini, H., Carrica, P., Kim, H., Toda, Y., Stern, F., 2010. URANS simulation and validation of added resistance and motions of the KVLCC2 crude Carrier with fixed and free surge conditions, Gothenburg 2010. A Workshop on CFD in Ship Hydrodynamics 517–522.
- Sadat-Hosseini, H., Wu, P., Carrica, P., Kim, H., Toda, Y., Stern, F., 2013. CFD verification and validation of added resistance and motions of KVLCC2 with fixed and free surge in short and long head waves. Ocean Eng. 59, 240–273.
- Salvesen, N., Tuck, E.O., Faltinsen, O.M., 1970. Ship Motions and Sea Loads SNAME, vol. 104, pp. 119–137.
- Seo, M.-G., Kim, K.-H., Park, D.-M., Kim, Y., 2013. Comparative study on added resistance for different hull forms by using weakly-nonlinear seakeeping formulations. J. Society of Naval Arch. Korea 50 (1), 49–58.
- Seo, M.-G., Yang, K.-K., Park, D.-M., Kim, Y., 2014. Numerical analysis of added resistance on ships in short waves. Ocean Eng. 87, 97–110.
- Shen, Z., Wan, D., 2013. RANS computations of added resistance and motions of a ship in head waves. Int. J. Offshore Polar Eng. 23 (04), 264–271.
- SHOPERA, 2016. Energy Efficient Safe Ship Operation EU FP-7 Project.
- SIMMAN, 2014. Workshop on Verification and Validation of Ship Manoeuvring Simulation Methods. Denmark.
- Stern, F., Xing, T., Yarbrough, D.B., Rothmayer, A., 2006. Hands-on CFD educational interface for engineering courses and laboratories. J. Eng. Educ. 95 (1), 63.
- Tezdogan, T., Demirel, Y.K., Kellett, P., Khorasanchi, M., Incecik, A., Turan, O., 2015. Full-scale unsteady RANS CFD simulations of ship behaviour and performance in head seas due to slow steaming. Ocean Eng. 97, 186–206.
- U.N., 2015. In: Nations, U. (Ed.), United Nations Framework Convention on Climate Change. Paris.
- Van't Veer, A.P., 2009. PRECAL v6.5 Theory Manual.